



OPEN ACCESS

EDITED BY

Niravkumar J. Joshi,
University of Barcelona, Spain

REVIEWED BY

Anjali Suresh,
ASM America, Inc., United States
Akshara Parekh,
Virginia Tech, United States

*CORRESPONDENCE

Bo Peng,
✉ pengbo@xhcom.edu.cn
Xiaohua Xie,
✉ xiexiaoh6@mail.sysu.edu.cn

RECEIVED 21 December 2023

ACCEPTED 31 January 2024

PUBLISHED 15 February 2024

CITATION

Chen C, Chen Z, Luo H, Peng B, Hao Y, Xie X,
Xie H and Li X (2024), Increasing the sensor
channels: a solution for the pressing offsets that
cause the physiological parameter inaccuracy
in radial artery pulse signal acquisition.
Front. Bioeng. Biotechnol. 12:1359297.
doi: 10.3389/fbioe.2024.1359297

COPYRIGHT

© 2024 Chen, Chen, Luo, Peng, Hao, Xie, Xie
and Li. This is an open-access article distributed
under the terms of the [Creative Commons
Attribution License \(CC BY\)](https://creativecommons.org/licenses/by/4.0/). The use,
distribution or reproduction in other forums is
permitted, provided the original author(s) and
the copyright owner(s) are credited and that the
original publication in this journal is cited, in
accordance with accepted academic practice.
No use, distribution or reproduction is
permitted which does not comply with these
terms.

Increasing the sensor channels: a solution for the pressing offsets that cause the physiological parameter inaccuracy in radial artery pulse signal acquisition

Chao Chen¹, Zhendong Chen¹, Hongmiin Luo², Bo Peng^{3,4*},
Yinan Hao³, Xiaohua Xie^{1*}, Haiqing Xie⁵ and Xinxin Li⁶

¹School of Computer Science and Engineering, Sun Yat-Sen University, Guangzhou, China, ²Science and Technology Innovation Center, Guangzhou University of Chinese Medicine, Guangzhou, China, ³Department of Musical Instrument Engineering, Xinghai Conservatory of Music, Guangzhou, China, ⁴Snow Research and Development Laboratory, Foshan, China, ⁵School of Medical Engineering, Foshan University, Foshan, China, ⁶School of Nursing, Sun Yat-Sen University, Guangzhou, China

Introduction: In studies of pulse wave analysis, single-channel sensors only adopt single temporal pulse signals without spatial information to show pulse-feeling patterns. Multi-channel arterial pulse signals, also named as three-dimensional pulse images (3DPis), provide the spatial and temporal characteristics of radial pulse signals. When involving single or few-channel sensors, pressing offsets have substantial impacts on obtaining inaccurate physiological parameters like tidal peak (P_2).

Methods: This study discovers the pressing offsets in multi-channel pulse signals and analyzes the relationship between the pressing offsets and time of P_2 (T_2) by qualifying the pressing offsets. First, we employ a data acquisition system to capture 3DPis. Subsequently, the $errorT_2$ is developed to qualify the pressing offsets.

Results: The outcomes display a central low and peripheral high pattern. Additionally, the $errorT_2$ increase as the distances from the artery increase, particularly at the radial ends of the blood flow direction. For every 1 mm increase in distances between sensing elements and center sensing elements, the $errorT_2$ in the radial direction escalates by 4.87%. When the distance is greater than 3.42 mm, the $errorT_2$ experiences a sudden increase.

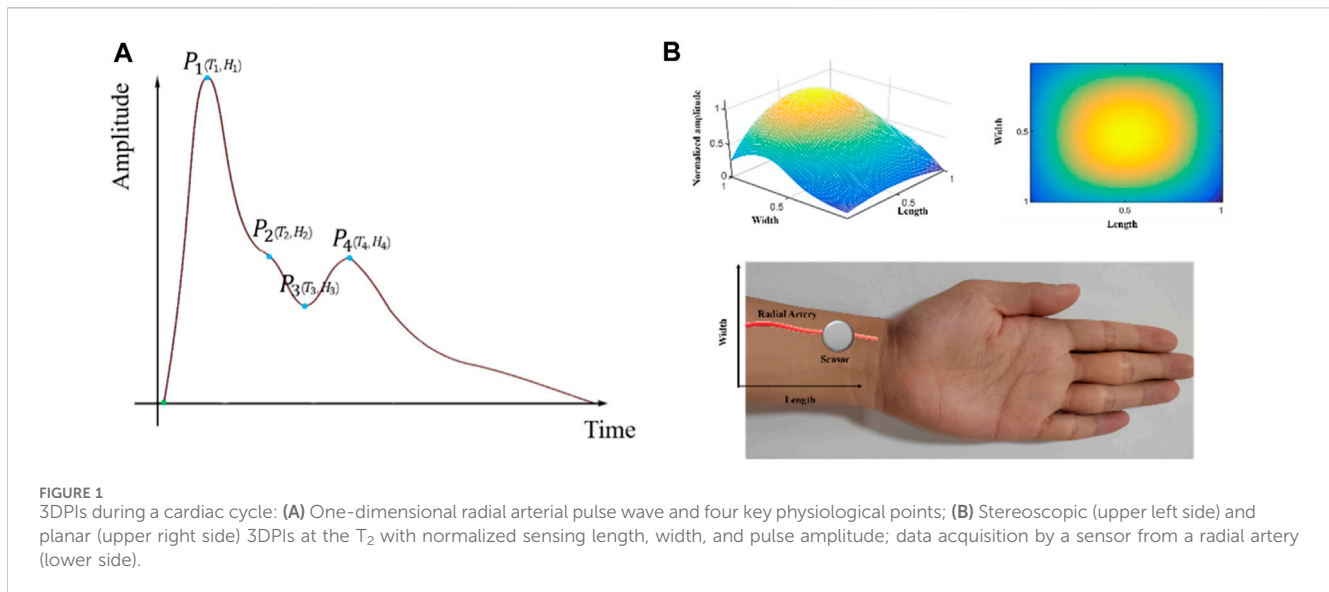
Discussion: The results show that increasing the sensor channels can overcome the pressing offsets in radial pulse signal acquisition.

KEYWORDS

multi-channel pulse signals, tactile sensors, tidal peak, pulse wave analysis, biomedical engineering

1 Introduction

Cardiovascular diseases (CVD) are the primary causes of death globally (Visseren et al., 2021). Pulse waves are generated by cardiac ejection during heart cycles and play a significant role in cardiovascular health. Pulse wave analysis (PWA), considered an essential diagnostic tool for assessing cardiovascular disease, detects early pathological modifications, such as arterial stiffness and endothelial dysfunction (AlGhatrif et al., 2013; Matsuzawa et al., 2015; Francque et al., 2016; Ohkuma et al., 2017; Chen et al., 2021). The roles of PWA in the diagnosis of CVDs



encompass the assessment of arterial stiffness, pulse wave velocity analysis, and pulse waveform analysis. Several physiological parameters, such as the peripheral augmentation index (pAIx), pulse transit time (PTT), reflection magnitude (RM), and reflection index (RI), are employed in PWA (Munir et al., 2008; Wang et al., 2010; Milicevic et al., 2020; Yao et al., 2022; Campitelli et al., 2023). The tidal peak (P_2), representing the second wave peak of the pure radial arterial pulse signals within a cardiac cycle, is one of the four key physiological points, which also include percussion peaks (P_1), diastolic notches (P_3), and diastolic peaks (P_4) (Su et al., 2016). These points represent key temporal markers within each cardiac cycle, conveying essential information about cardiovascular health. The P_2 reflects the pressure wave originating from peripheral resistance vessels, which reflects the amplitudes of arterial stiffness and is crucial in the assessment of arterial stiffness (Peng et al., 2022; Chen et al., 2023). Figure 1A illustrates the positions of the four key physiological points during a cardiac cycle.

To measure radial pulse signals, a series of acquisition devices have been developed and applied in pulse acquisition (Luo et al., 2012a; Qiao et al., 2018; Tsai et al., 2018; Fu et al., 2019; Huang et al., 2019). These devices employ sensors with one sensing element to capture radial pulse signals. However, these single-channel sensors only adopt single temporal pulse signals without spatial information to show pulse-feeling patterns (Kim et al., 2011; Kim et al., 2012; Huang et al., 2019). In recent years, multi-channel pulse signals have been widely measured using tactile sensors for pulse signal application studies (Chung et al., 2011; Kong et al., 2016; Peng et al., 2019; Zhang et al., 2021; Liu et al., 2023). The multi-channel arterial pulse signals, also named as three-dimensional pulse images (3DPIs), provide the three-dimensional spatial and temporal characteristics of pulse signals (Peng et al., 2019). 3DPIs also enhances the visualization of pulse signals and provides more cardiovascular-related information. During data acquisition, 3DPIs at T_2 (time of P_2) are often focal points of interest (Cui et al., 2019; Yuen et al., 2019; Luo et al., 2021). Figure 1B displays the stereoscopic/planar 3DPIs at the T_2 and data acquisition by a sensor from a radial artery. Most devices for obtaining 3DPIs fix the tactile sensors, which are a kind of multi-channel sensors, on the robotic finger and control the robotic finger to press on the position of radial arteries to

acquire the pulse signals (Chung et al., 2011; Si et al., 2011; YF et al., 2011; Luo et al., 2012a; Luo et al., 2012b; Chung et al., 2012; Hu et al., 2012; Chung et al., 2013; Luo and Chung, 2016; Luo et al., 2016; Luo et al., 2018; Peng et al., 2019).

During the pressing process, the T_2 are different in all channels of the tactile sensors (Peng et al., 2019). However, in scenarios involving sensors with one or few sensing elements, pressing offsets are inevitable. In such cases, the operators may face difficulties in judging whether the pressing process is accompanied by offsets since the sensitivities of single-channel sensors are not uniform (Dario and Bergamasco, 1988; Dario and Buttazzo, 2016; Fearing, 2016). Subsequently, operators may encounter challenges in obtaining multi-channel pulse signals that reflect true arterial conditions. Then, operators may obtain inaccurate physiological parameters like T_2 . Operators encounter a challenge when detecting pressing offsets during the acquisition of multi-channel pulse signals due to the lack of appropriate quantitative tools for this purpose. By detecting whether any offsets occur during the pressing process, operators can adjust the pressing position to ensure the acquisition of 3DPIs that accurately reflect the arterial conditions.

This study discovers the pressing offsets in multi-channel pulse signals and analyzes the relationship between the pressing offsets and T_2 by qualifying the pressing offsets in pulse signal acquisition. First, we employ a data acquisition system to capture 3DPIs from the subjects. Then, the errors between each channel and the best channel in 3DPIs are determined to qualify the pressing offsets in the tactile sensor. Finally, the subjects are divided into multiple control groups, and the results are compared and analyzed. Due to the high sensitivity and mature fabric technologies, operators prefer to employ tactile sensors to obtain pulse signals (Yang et al., 2017). In this study, we employ the tactile sensors developed by PPS (Pressure Profile Systems Inc., Los Angeles, CA, United States), which are widely recognized as the preferred choice for acquiring physiological signals across a diverse range of clinical environments (Cui et al., 2019). PPS tactile sensors are designed with exceptional sensitivity and accuracy to detect tiny changes in pressure that are indicative of pulse signals. Electrodes as sensing elements are arranged in orthogonal, overlapping strips to create a tactile sensor. The electrodes overlap at each position to form a

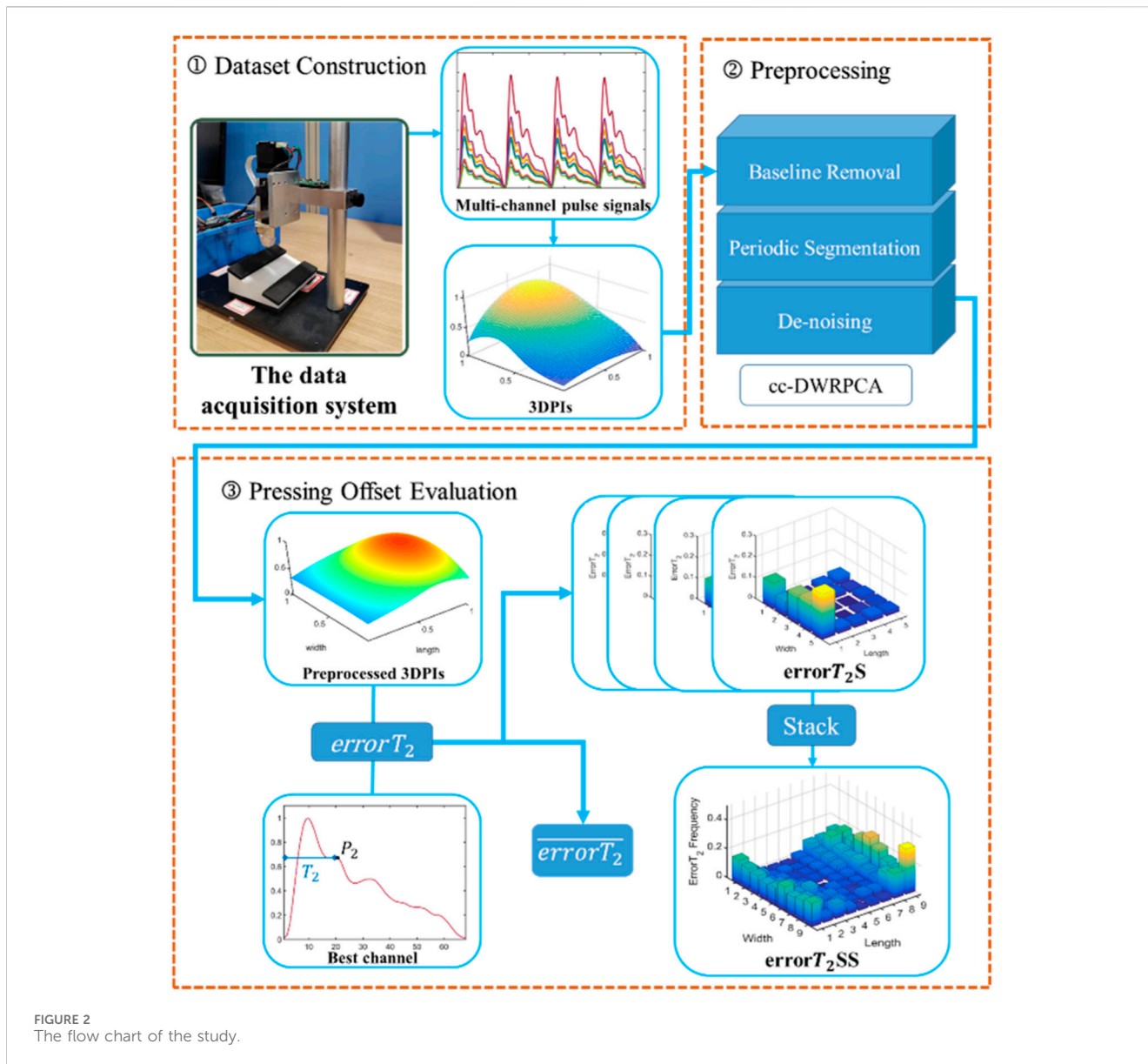


FIGURE 2 The flow chart of the study.

TABLE 1 Subject characteristics in this study (Mean ± Standard Deviation).

	All	Male	Female
Number	52	44	8
Age (year)	59.98 ± 14.94	59.64 ± 15.47	61.88 ± 15.47
Height (cm)	164.25 ± 7.48	165.59 ± 6.673	156.88 ± 6.67
Weight (kg)	72.17 ± 12.91	72.45 ± 12.97	70.63 ± 12.97
BMI (kg/m ²)	26.68 ± 4.00	26.32 ± 3.77	28.67 ± 3.77
Systolic BP (mmHg)	136.96 ± 23.59	135.70 ± 21.25	143.88 ± 21.25
Diastolic BP(mmHg)	80.17 ± 14.03	81.20 ± 13.70	74.50 ± 13.70
Heart rate (beats/min)	69.54 ± 10.30	70.39 ± 9.12	64.88 ± 9.12

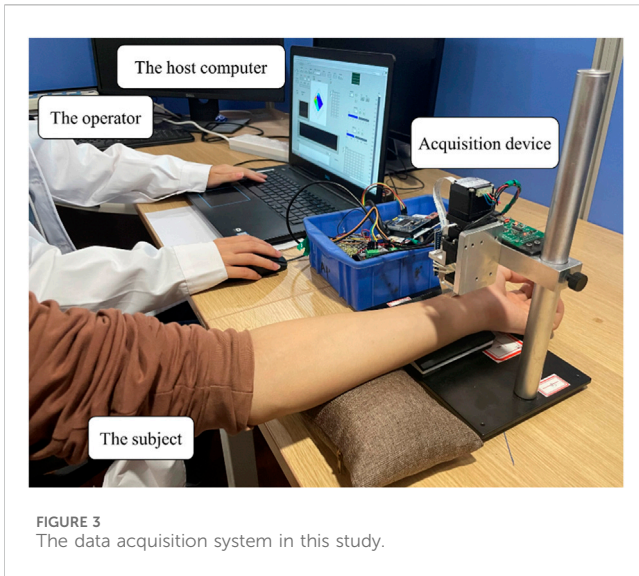
discrete capacitor. A single row and column are selectively scanned to determine the capacitance and pressure (Hu et al., 2012). PPS sensors offer the ability to customize tactile sensors to meet specific research or

clinical needs, thus PPS sensors come in a variety of specifications. In this article, a PPS sensor with 5 rows and 5 columns is denoted as a 5 × 5 sensor. The 5 × 5-1 PPS sensor can provide a tactile center point by positioning the blank area in the corner (Peng et al., 2019).

The rest of this paper is organized as follows. In Methods section, data construction, preprocessing, and pressing offset evaluation are introduced. The Results section illustrates the results of different control groups. Lastly, the final section concludes with a discussion of the experimental results.

2 Materials and methods

Figure 2 presents a comprehensive depiction of the entire workflow, consisting of three primary stages: dataset construction, preprocessing, and pressing offset evaluation. The dataset construction section involves utilizing a multi-channel pulse acquisition device to capture pulse signals from the subjects. Subsequently, the acquired pulse wave dataset



employ two strategies to ensure the accurate acquisition of 3DPs. We utilize a specialized pulse signal acquisition device, which include PPS sensors, the most popular tactile sensors, and follow stringent data collection protocols. A PPS sensor, a fixture, a robotic finger, a stepper motor (to control the pressing depth of the robotic finger), and a main control board make up the uniaxial device (Figure 3). This study utilizes a PPS tactile sensor with an 85 Hz sampling rate. The rectangular geometry of a sensing element in the PPS tactile sensor is 1.25×1.71 mm (Peng et al., 2019). The main control board, based on STM32 (Jin et al., 2019), is responsible for managing the underlying hardware, collecting PPS data, and establishing serial port communication with the host computer. Pulse signals are detected using a 24-channel PPS tactile sensor. Subjects are scheduled to sit in a chair in a quiet room for a minimum of 10 min before their pulse signals are recorded. The operator can easily handle the computer and oversee the measurement process while the subject is comfortably tested on their wrist at the same height as their heart due to their proper relative locations. The data collection process adheres strictly to the protocol established in our previous research (Peng et al., 2019).

undergoes preprocessing, which includes baseline removal, periodic segmentation, and de-noising. Finally, the preprocessed data is then utilized for calculating the $\overline{errorT_2}$ and facilitating the construction of $errorT_2SS$.

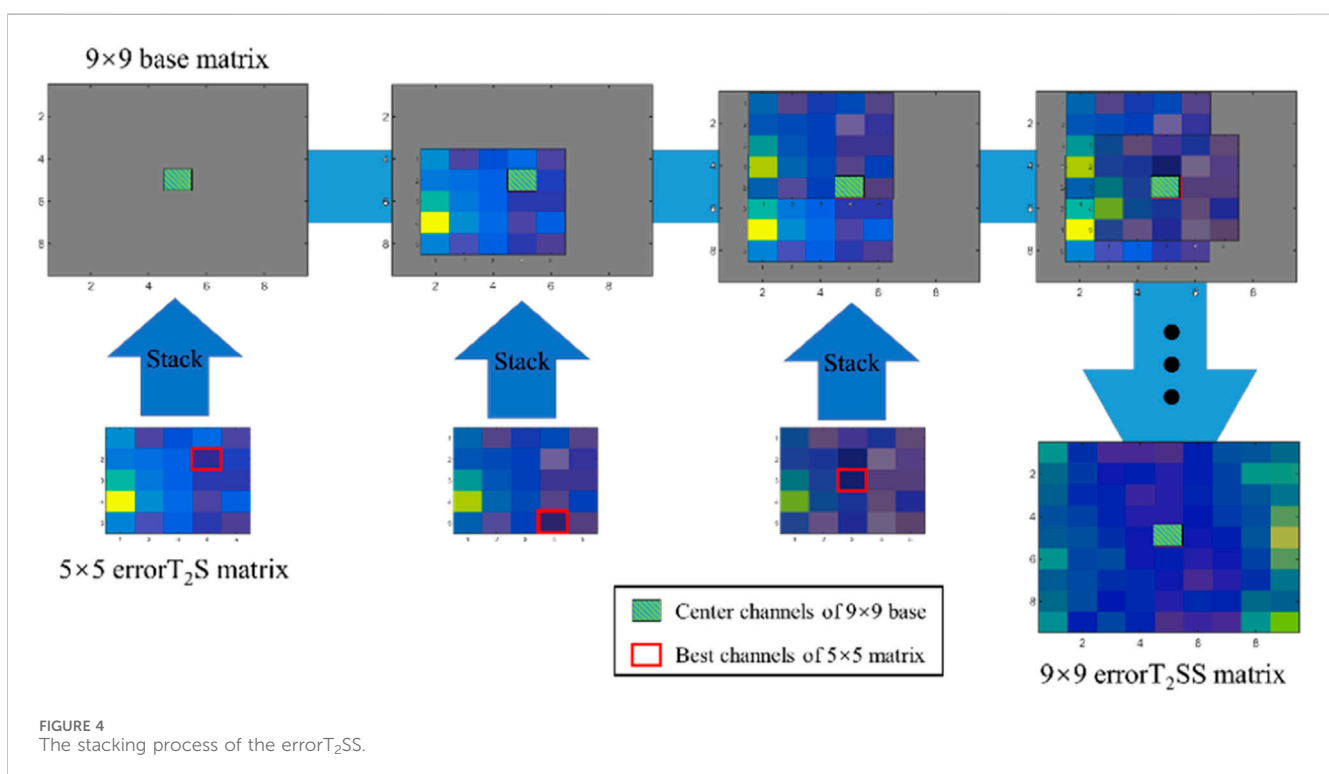
2.1 Dataset construction

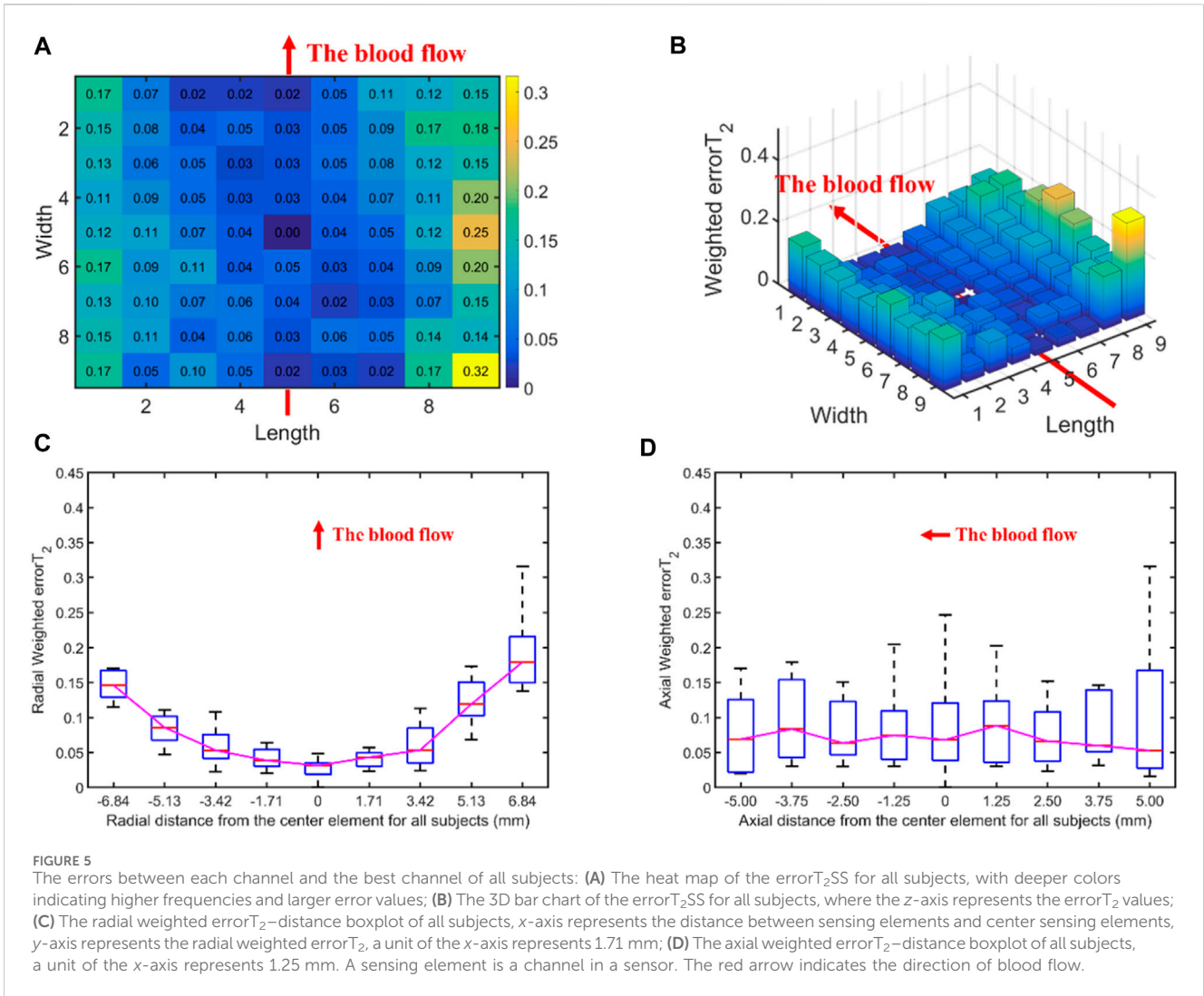
2.1.1 Data acquisition

This study employs a data acquisition system for capturing pulse signals from subjects. In the data acquisition system of this study, we

2.1.2 Subjects and control groups

The institutional review board at the National Cheng Kung University Hospital granted authority for this study to conduct a human trial (Approval Number: B-ER-103-263). The collected personal data from 52 subjects, with sequentially acquired valid data for both hands, is examined and analyzed (Table 1). Among the subjects, 15 are non-hypertensive subjects, and 37 are hypertensive patients. Finally, 623 multicycle pulse signal samples with 24 channels ($5 \times 5-1$) are acquired. In this study, the subjects are divided into three control groups: left hands/right hands, male/female, and non-hypertensive/hypertensive.





2.2 Preprocessing

Numerous studies have employed a thorough and suggested pulse signal pipeline to preprocess pulse signals (Wang et al., 2016; Peng et al., 2019; Peng et al., 2022; Song et al., 2023). In this section, a complete preprocessing pipeline includes baseline removal, periodic segmentation, and de-noising.

First, to eliminate baseline wandering from the signals, a first-order Butterworth high-pass filter with a cut-off frequency of 0.5 Hz is applied (Li, 2007). Second, the multi-channel signals are segmented into individual single-period pulse signals for the de-noising demand of the subsequent algorithm. Finally, a de-noising algorithm called Cross-Channel Dynamic Weighting Principal Component Analysis (cc-DWRPCA) is implemented to de-noise the processed pulse signals (Peng et al., 2022).

The cc-DWRPCA, based on Robust Principal Component Analysis (RPCA) (Candès et al., 2011), employs a channel-scaled factor (CSF) technique to manipulate the weights ω among channels (see Eq. 1), which can get superior performances than weighted robust principal component analysis (WRPCA) (He et al., 2019). Without using the inherent correlations between these channels, WRPCA is able to extract signal properties for each channel

independently. After de-noising with cc-DWRPCA, 623 single-cycle pulse signals with $5 \times 5-1$ are extracted.

$$\omega_c = \frac{\eta}{\sigma_c(D) + \epsilon}, \tag{1}$$

where ω_c is the weight of the c th channel of a subject, η denotes the c th CSF of D in the c -th channel, $\sigma_c(D)$ represents c th singular value of D , D is the singular value decomposition of a multicycle pulse signal, ϵ is the reconstruction error tolerance, which is set to $1e-6$ in this study.

To obtain a complete 5×5 matrix, we employed interpolation to generate an additional channel for each sample, transforming the $5 \times 5-1$ matrix (24 channels) into a 5×5 matrix (25 channels). Consequently, a complete 5×5 3DPI is available for each sample. Eq. 2 shows the arrangement of a 5×5 tactile sensor.

$$\begin{pmatrix} 1 & 6 & 11 & 16 & 21 \\ 2 & 7 & 12 & 17 & 22 \\ 3 & 8 & 13 & 18 & 23 \\ 4 & 9 & 14 & 19 & 24 \\ 5 & 10 & 15 & 20 & 25 \end{pmatrix}, \tag{2}$$

where the numbers in the matrix represent the numbers of channels.

TABLE 2 $\overline{errorT_2}$ on different control groups.

	$\overline{errorT_2}$
All subjects	0.058 ± 0.061
Left hands	0.053 ± 0.052
Right hands	0.065 ± 0.068
Male	0.059 ± 0.060
Female	0.057 ± 0.067
Non-hypertensive subjects	0.052 ± 0.048
Hypertensive subjects	0.060 ± 0.063

2.3 Pressing offset evaluation

In this article, the errors between each channel and the best channel in 3DPs are determined to evaluate the pressing offsets. Following preprocessing, channels with the maximum amplitude are automatically selected as the best channels for each sample. Using these best channels as a benchmark, a stringent manual screening of the samples is conducted by a cardiovascular expert, who also provided manual annotations for the P_2 position. The expert annotation serves as the gold standard for P_2 localization. In this section, $errorT_2$, the average $errorT_2$ ($\overline{errorT_2}$), and $errorT_2$ Stacked Surface ($errorT_2SS$) are proposed to evaluate the pressing offsets.

By performing manual annotations for P_2 , the T_2 across all channels are obtained for each sample. Subsequently, for each sample, the error between each channel and the maximum channel, representing the $errorT_2$ for each channel, are calculated (see Eq. 3). Then, $\overline{errorT_2}$ across all channels for all subjects are calculated (see Eq. 4). Based on the specifications of the 5×5 tactile sensors, we arrange the $errorT_2$ of 25 channels and ultimately obtain the $errorT_2$ Surface ($errorT_2S$) matrix for each sample. The $errorT_2$ can assess the discrepancy between T_2 of a single channel and the best channel, while $errorT_2S$ evaluates the pressing offset for a sample. $errorT_2S$ can also assess the discrepancy between T_2 of each channel and the best channel in the spatial domain, thereby facilitating an understanding of the distribution of pulse extraction center points.

$$errorT_2(n, c) = |T_{2c}(n) - T_{2best}(n)|, \quad (3)$$

where c represents the number the channel, $T_{2c}(n)$ is T_2 in the c th channel of sample n , $T_{2best}(n)$ is T_2 in the best channel of sample n .

$$\overline{errorT_2}(n) = \frac{\sum_c^{\Gamma} |T_{2c}(n) - T_{2best}(n)|}{\Gamma}, \quad (4)$$

where Γ is 25, the number of all channels in this study.

To investigate the offset degree of the robotic finger pressing process during data collection, the $errorT_2S$ of all samples are stacked to construct the $errorT_2SS$. Algorithm 1; Figure 4 demonstrate the construction process of the $errorT_2SS$. Firstly, a 9×9 zero matrix is created to represent the 9×9 channel matrix as the base. Subsequently, the best channels of each $errorT_2S$ are aligned with the center channel of the base for stacking. Lastly, the weighted $errorT_2$ are calculated for each channel within the 9×9 base (see Eqs 5, 6). The obtained weighted $errorT_2$ constitute the $errorT_2SS$ matrix.

$$Weighted\ errorT_2(c) = \sum_n^N \omega_n \cdot errorT_2(n, c), \quad (5)$$

ω_n represents the weight in c th channel, which is defined as:

$$\omega_n = \begin{cases} 1, & errorT_2(n, c)_{9 \times 9} > 0 \\ 0, & errorT_2(n, c)_{9 \times 9} = 0 \end{cases}, \quad (6)$$

where $errorT_2(n, c)_{9 \times 9}$ denotes the c th $errorT_2$ that $errorT_2S$ of a sample is stacked and aligned to the center channel of the 9×9 base.

Input: T_2 : time of P_2 ;

S : pulse signals, S_c is the pulse signal of the c th channel;

N : number of samples, n is the n th sample;

M : Arrangement of the 5×5 tactile sensor

Output: $errorT_2SS$: $errorT_2$ Stacked Surface matrix

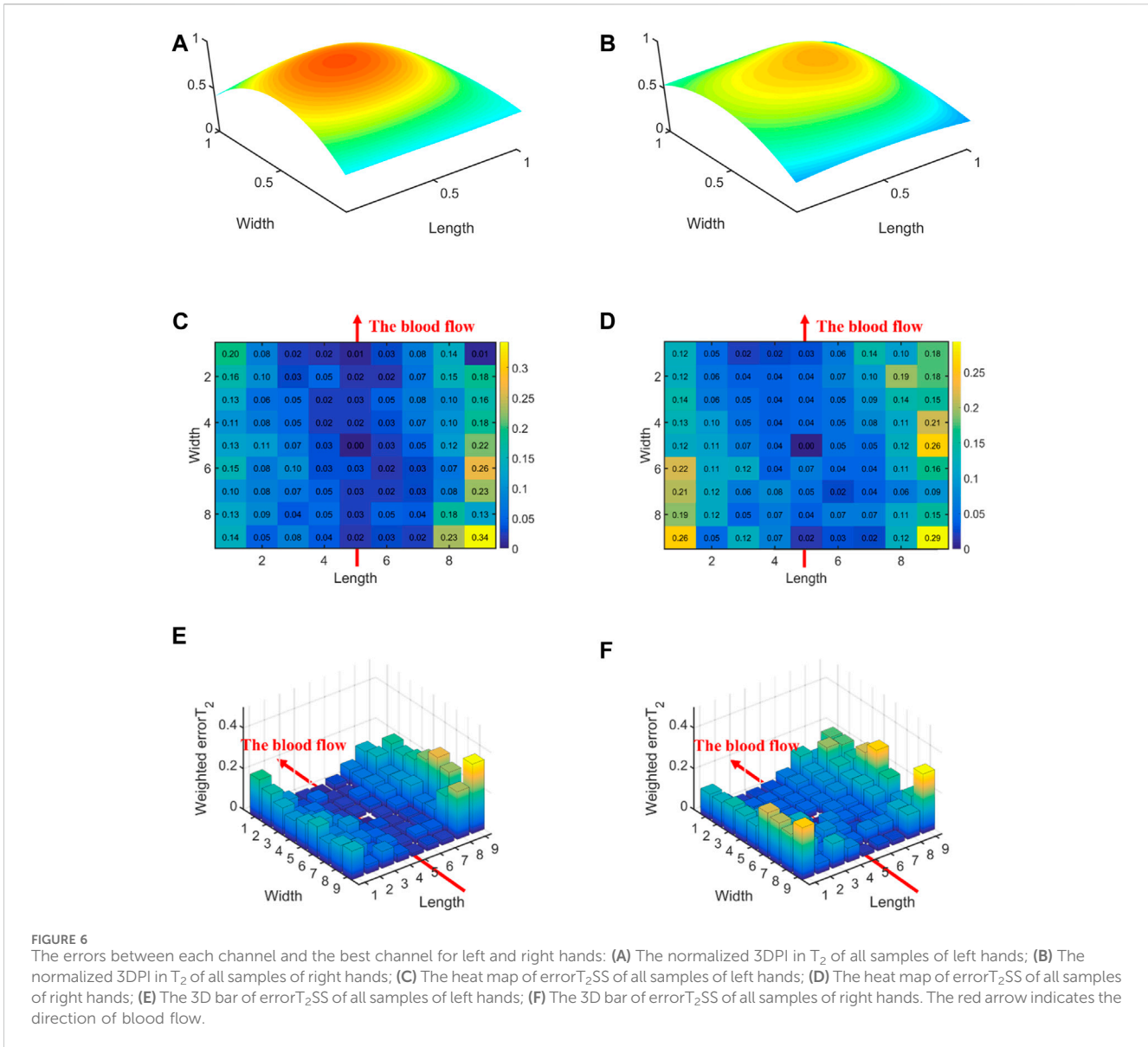
- 1: Initialize an empty $errorT_2$ Surface ($errorT_2S$) matrix
- 2: **for** each sample **in** n **do**
- 3: extract channel with maximum amplitude as $S_{best}(n)$
- 4: **for** each channel in all channels of sample n **do**
- 5: calculate $errorT_2$ for $S_c(n)$ using Eq. 3
- 6: **end for**
- 7: arrange all $errorT_2(c)$ of 25 channels according to M to form $errorT_2S(n)$
- 8: **end for**
- 9: Initialize a 9×9 zero matrix as base
- 10: **for** each $errorT_2S(n)$ **do**
- 11: align best channels with the center channel of the base
- 12: stack the aligned $errorT_2S(n)$ on top of the base
- 13: **end for**
- 14: calculate the weighted $errorT_2$ for each channel using Eq. 5
- 15: form $errorT_2SS$ matrix using the weighted $errorT_2$

Algorithm 1. Construction process of the $errorT_2SS$.

3 Results

3.1 Quantitative analysis of all subjects

Figure 5 displays the $errorT_2SS$ and weighted $errorT_2$ -distance relation for all subjects. Figures 5A, B present the heat map and 3D bar of the $errorT_2SS$ for all subjects, respectively. The $errorT_2SS$ demonstrates a central low and peripheral high pattern. The further away from the center point, the higher the weighted $errorT_2$ trend. Furthermore, an upward trend is observed at both ends of the axis corresponding to the blood flow direction, with higher weighted $errorT_2$ as distance from the vessel increases. The central value is 0, as it represents that the central channel covers the best channels of all samples. Figures 5C, D illustrate the weighted $errorT_2$ -distance



boxplots for all subjects. The boxplots indicate nonlinear relationships between the increase in distance and the corresponding increase in $error_{T_2}$. For every 1 mm increase in distances between sensing elements and center sensing elements, the weighted $error_{T_2}$ in the radial direction escalates by 4.87%. The weighted $error_{T_2}$ tends to be stable in the axial direction. As the distances from the center channel increase, the volatilities of the $error_{T_2}$ become more pronounced. When the distance is greater than 3.42 mm, the radial weighted $error_{T_2}$ experiences a sudden increase.

Table 2 shows the $\overline{error_{T_2}}$ on different control groups in this study. In summary, the $\overline{error_{T_2}}$ of all subjects is 0.058. The $\overline{error_{T_2}}$ for left-handed subjects and non-hypertensive subjects are relatively lower, at 0.053 and 0.052. In comparison, right-handed subjects, males, and hypertensive subjects exhibit higher $\overline{error_{T_2}}$ of 0.065, 0.059, and 0.060, respectively. With regard to gender, male subjects have a slightly lower $\overline{error_{T_2}}$ than females, with values of 0.059 and 0.057.

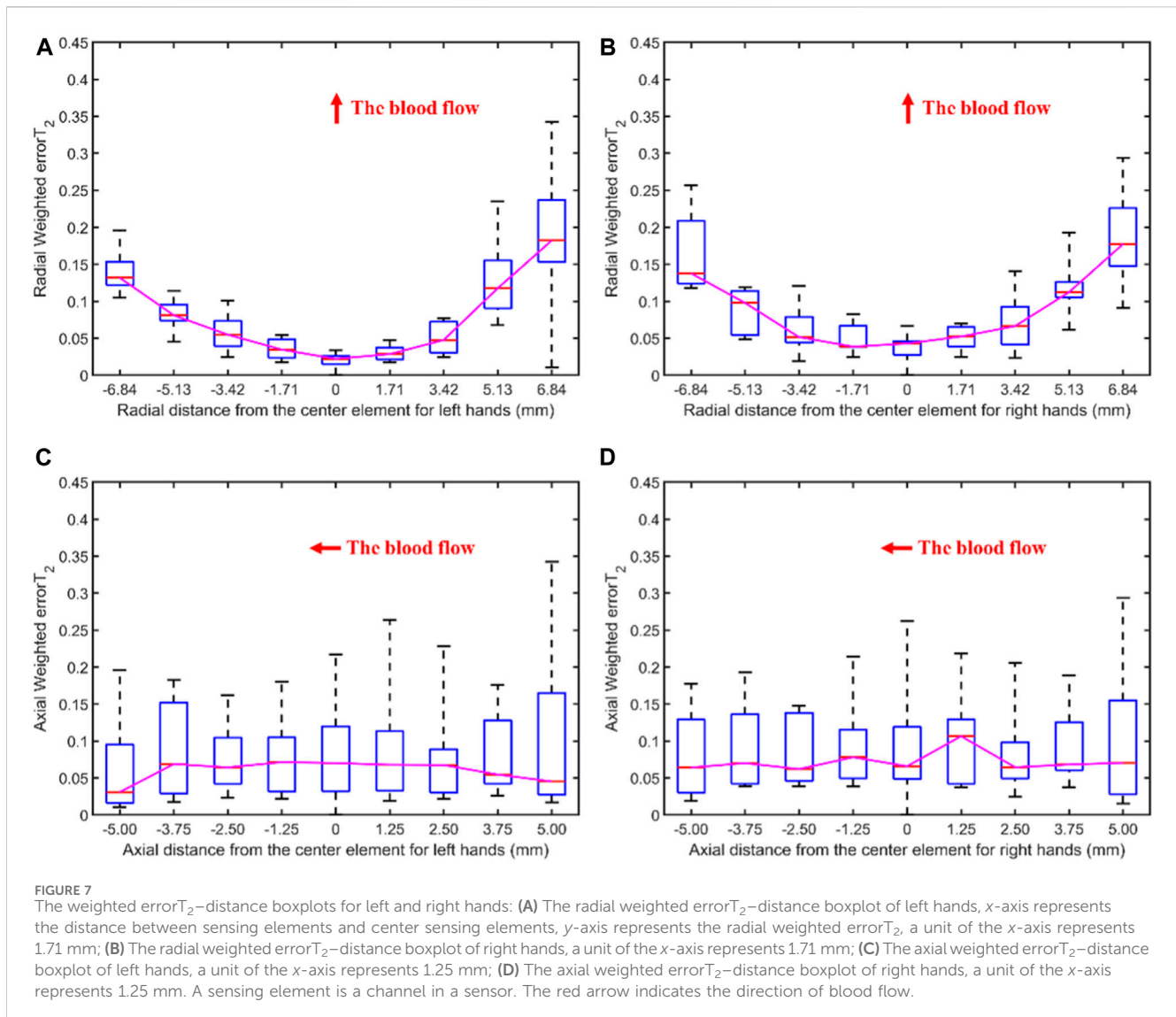
3.2 Comparative study for all control groups

3.2.1 Left hands vs. Right hands

Figure 6 displays the errors between each channel and the best channel of left and right hands. The $error_{T_2SS}$ exhibits a central low and peripheral high pattern for both hands. Moreover, an upward trend is observed at both ends of the axis corresponding to the blood flow direction. It can be observed that the error distributions for both hands show a subtle difference compared to the average error (Figure 5) distribution for all subjects. The boxplots in Figure 7 indicate that for every 1 mm increase in distance, the weighted $error_{T_2}$ in the radial direction for left and right hands escalate by 4.55% and 5.04%, respectively. When the distance is greater than 3.42 mm, the radial weighted $error_{T_2}$ for the left and right hands experience sudden increases.

3.2.2 Male vs. Female

Figure 8 illustrates the errors between each channel and the best channel of male and female subjects. The $error_{T_2SS}$ shows a central



low and peripheral high pattern for both male and female, with an upward trend at both ends of the axis corresponding to blood flow direction. It is noteworthy that the right-most channels of the error_{T₂}SS for female samples exhibit data missing, suggesting that no channels were stacked on the base channels during the stacking of error_{T₂}S for female subjects. The weighted error_{T₂} in the upper-right corner of the error_{T₂}SS for females are relatively greater, which may be caused by outlier values. Figure 9 shows that for every 1 mm increase in distance, the weighted error_{T₂} in the radial direction for male and female subjects rise by 4.86% and 3.98%, respectively. When the distance is greater than 3.42 mm, the radial weighted error_{T₂} for the male subjects experiences a sudden increase. Since the data in the right-most channels is missing, there are only 8 distance groups in Figure 9B.

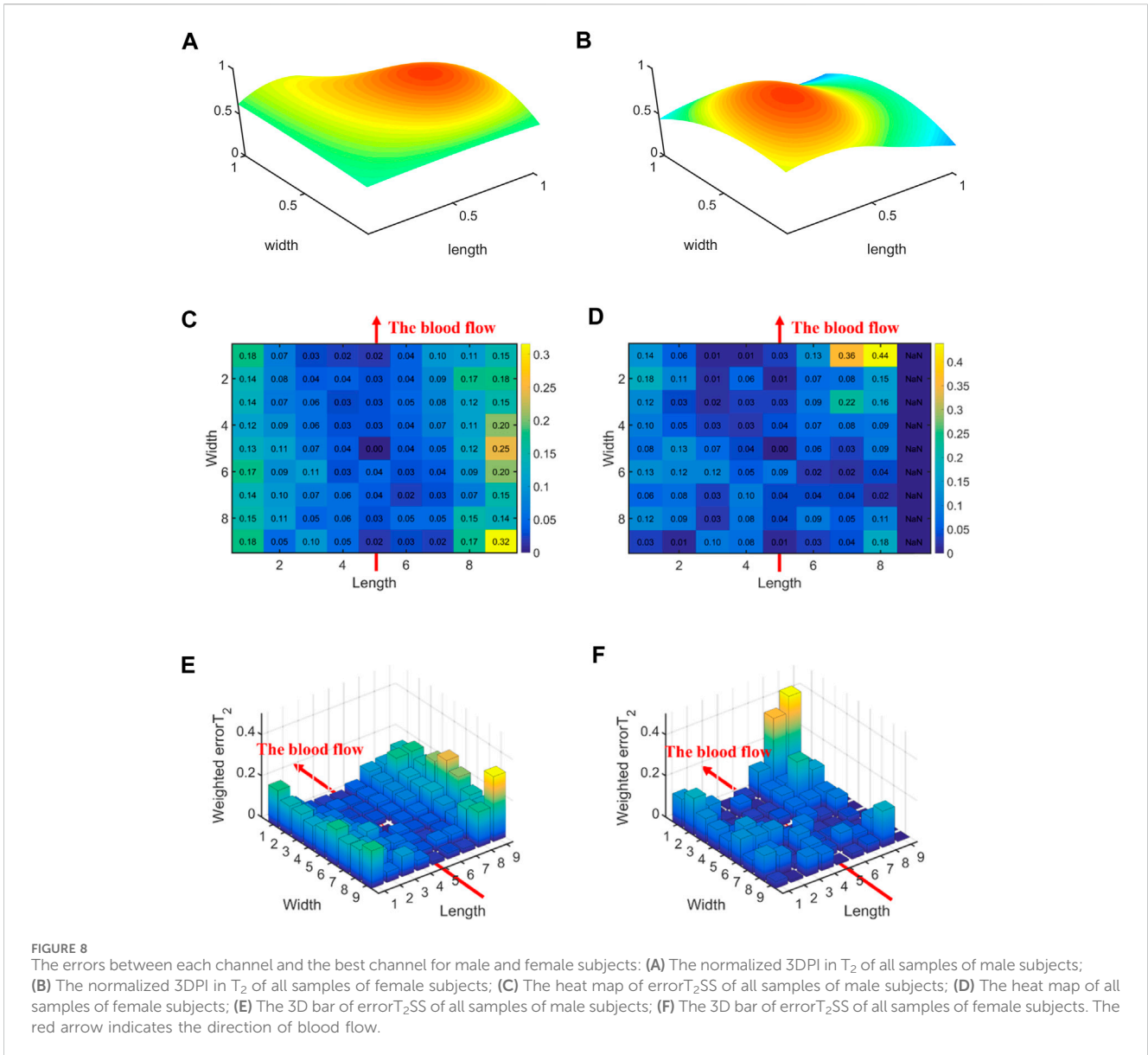
3.2.3 Non-hypertensive vs. Hypertensive

Figure 10 displays the errors between each channel and the best channel for non-hypertensive and hypertensive subjects. The error_{T₂}SS exhibits a pattern of central decrement and peripheral increment, with an ascending trend at both extremities of the axis

corresponding to the direction of blood flow. It can be inferred that the error_{T₂}SS for non-hypertensive subjects is more evenly distributed compared to hypertensive patients overall, whereas the error_{T₂}SS for hypertensive patients exhibits smaller errors along the arterial axis. Figure 11 indicates that for every 1 mm increase in distance, the weighted error_{T₂} in the radial direction for non-hypertensive and hypertension subjects rise by 4.94% and 5.04%, respectively. When the distance is greater than 3.42 mm, the radial weighted error_{T₂} for the non-hypertensive and hypertension subjects experience sudden increases.

4 Discussion

This study discovers the pressing offsets in multi-channel pulse signals and analyzes the relationship between the pressing offsets and T₂ by qualifying the pressing offsets in pulse signal acquisition. First, we employ a data acquisition system to obtain 3DPIS from the subjects. Subsequently, the errors between each channel and the best channel are determined. The error T₂ Stacked Surface (error_{T₂}SS)

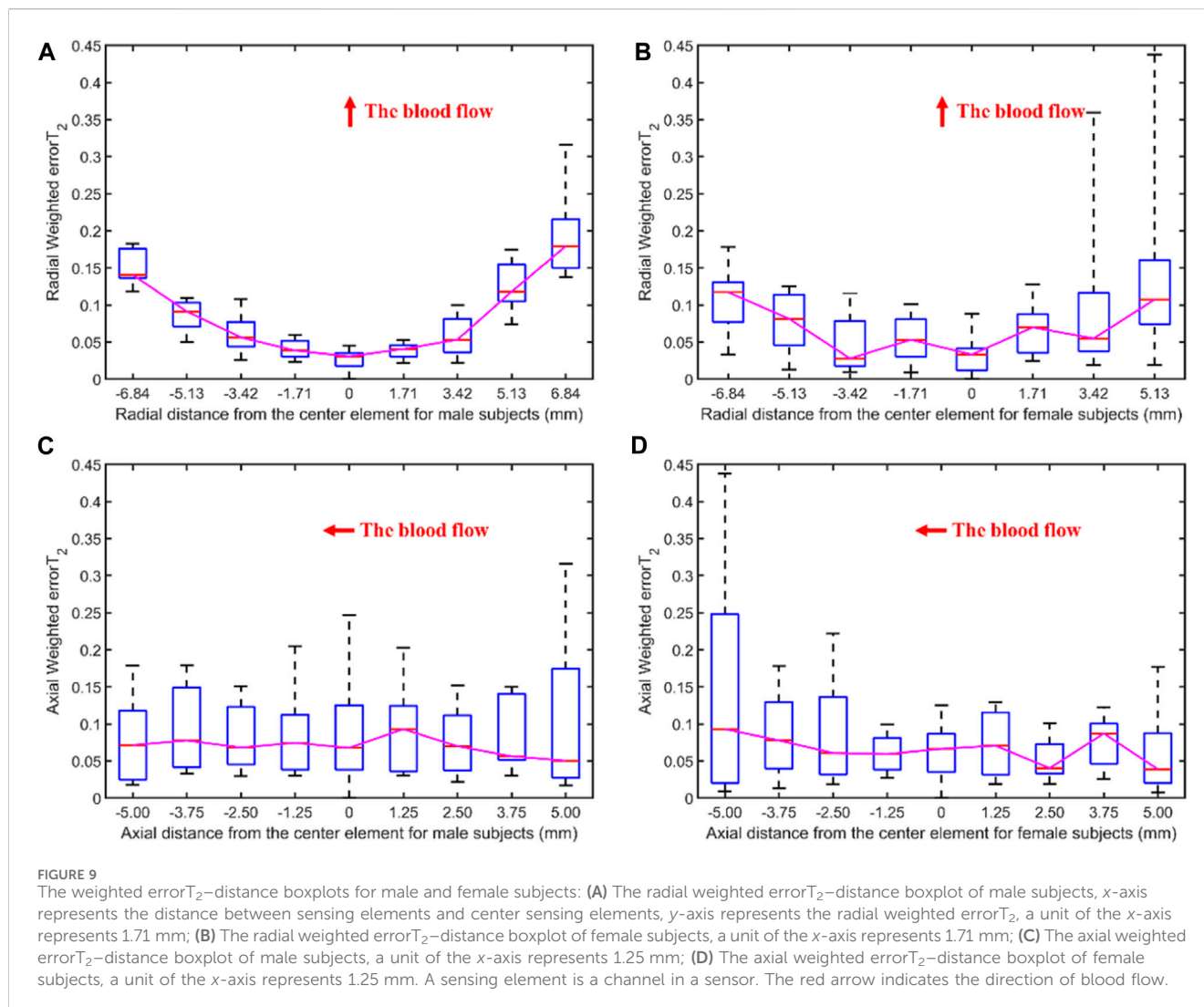


and the average error T_2 ($\overline{errorT_2}$) are implemented to qualify the pressing offsets in the tactile sensor. Finally, the subjects are divided into multiple control groups, and the results are compared and analyzed.

Figures 5, 6, 8, 10 display the error between each channel and the best channel for all control groups. All $errorT_2SS$ in these figures exhibit a central low and peripheral high pattern. In each $errorT_2SS$, the further away from the central point, the more upward the trend for all channels. The comparative study shows similar patterns for all subjects and control groups, revealing that our qualifications meet the true conditions of arterial pulse signals and the characteristics of the human radial arteries. The center of each $errorT_2SS$ reflects the offsets of the best channels, which are the smallest among all channels. The positions of the best channels align with the center of pressure on the arteries. Furthermore, the error values increased as distance from the artery increased, particularly at the axial ends of the blood flow direction. In Figure 8, data missing is existed in the rightmost column of the $errorT_2SS$ for female subjects. Considering the

sample size of female subjects in this study, the $errorT_2S$ of female samples may not thoroughly cover the entire 9×9 base matrix. Another possible reason is that the arteries of women exhibit more diminutive diameters (Xu et al., 2017; Deora et al., 2022) and are more difficult to adapt to the robotic fingertips. The inspiration from the results is selecting sensors with tiny sensing elements for pulse signal acquisition for female subjects. Figure 10 shows that the error distribution of non-hypertensive subjects is more uniform compared to hypertensive patients, while the $errorT_2SS$ of hypertensive patients has lower errors in the arterial axis. Compared to hypertensive patients, non-hypertensive subjects have lower vascular stiffness (Su et al., 2016; Zhang et al., 2021). Subsequently, during the pressing process of the robotic finger, the offsets might occur less.

The boxplots in Figures 7, 9, 11 indicate nonlinear relationships between the increase in distance and the corresponding increase in $errorT_2$. For every 1 mm increase in distances between sensing elements and center sensing elements, the weighted $errorT_2$ in the radial direction escalates by 4.87%. The weighted $errorT_2$ escalations for left hands/right



hands, male/female, and non-hypertensive/hypertensive are 4.55%/5.04%, 4.86%/3.98%, and 4.94%/5.04%, respectively. The clinical insights derived from these distinct results indicate that each clinical population possesses distinct physiological characteristics. Therefore, when acquiring pulse signals, it is essential to employ appropriate collection and measurement techniques to mitigate pressing offsets. For all control groups, when the distance is larger than 3.42 mm, the weighted radial error T_2 experience sudden increases for all subjects and control groups. This result can assist and guide operators in pressing processes. In clinical practice, we recommend the pressing offset of sensors not exceed 3.42 mm, which can adjust by qualifying the evaluation metrics. The weighted error T_2 tends to be stable in the axial direction. To our knowledge, the reason is that axial direction is the direction of the blood flow. The changes in the mechanical environment are different between axial and radial of the arterial smooth muscle (Messas et al., 2013; Rothermel et al., 2020).

When the robotic fingers of pulse acquisition devices apply pressing, offset may occur, potentially affecting measurement outcomes. In scenarios involving single or few-channel sensors, such offsets have more substantial impacts on measurement results. In such cases, the operators may face difficulties in establishing whether the

pressing process is accompanied by offsets. Such hindrance could potentially detract physicians from making accurate assessments of cardiovascular conditions in patients. This study detects pressing offsets in radial arterial pulse signals and explores the solution to prevent pressing offsets. In the analysis of this study, the error T_2 enables the quantification and evaluation of 3DPI, thus allowing for the determination of the offset degree during the pressing process and subsequent correction. With adequate sensor channels, we can implement the measurements in this study to qualify and evaluate the pressing offsets. However, when the number of sensor channels is one or few, it is hard to use the measurements to determine the pressing offset, and the operators face difficulties in establishing whether the pressing process is accompanied by offsets. Furthermore, only adequate sensor channels can help operators obtain more accurate clinical and physiological parameters, which are essential for the further assessment and diagnosis of physiological conditions in subjects. This is undoubtedly of great importance in clinical practice. Therefore, we highlight that increasing the sensor channels is crucial for achieving quantitative offset assessment.

Furthermore, the arterial conditions are compared and analyzed under different circumstances. This study employs three control groups:

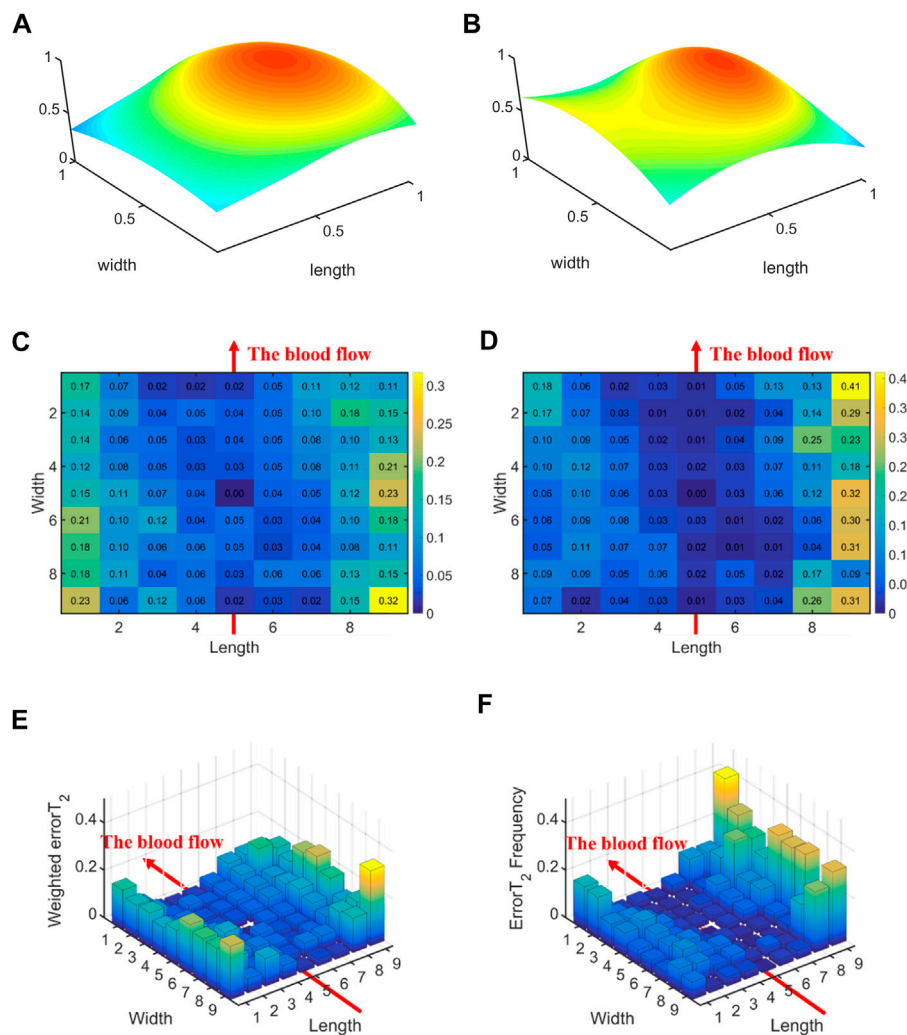


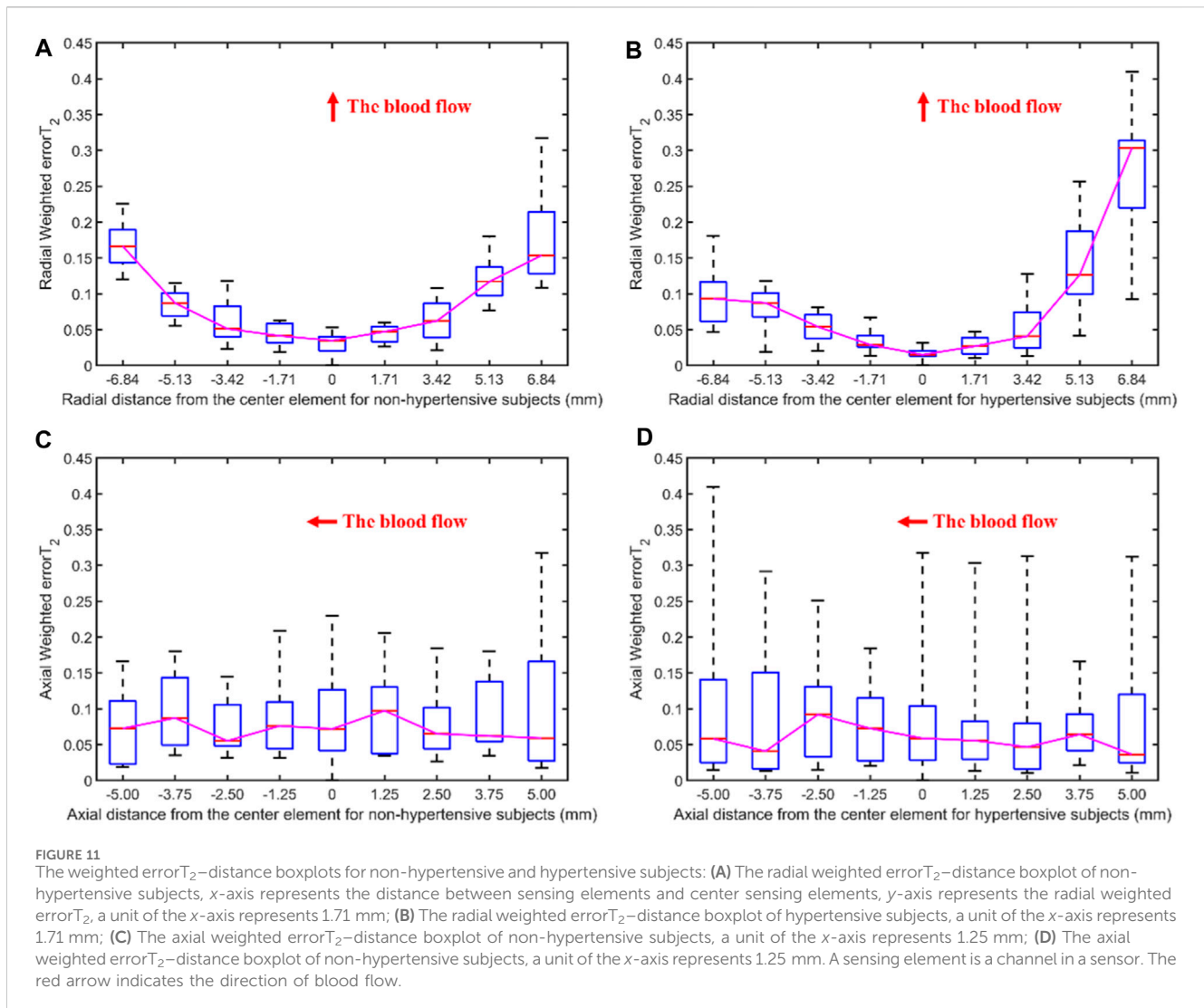
FIGURE 10
 The errors between each channel and the best channel for non-hypertensive and hypertension subjects: (A) The normalized 3DPI in T_2 of all samples of non-hypertensive subjects; (B) The normalized 3DPI in T_2 of all samples of hypertension subjects; (C) The heat map of $errorT_2SS$ of all samples of non-hypertensive subjects; (D) The heat map of $errorT_2SS$ of all samples of hypertension subjects; (E) The 3D bar of $errorT_2SS$ of all samples of non-hypertensive subjects; (F) The 3D bar of $errorT_2SS$ of all samples of hypertension subjects. The red arrow indicates the direction of blood flow.

left hands/right hands, male/female, and non-hypertensive/hypertensive subjects. During the pressing process, the tactile sensors of the pulse signal acquisition instrument are similarly influenced by the arteries of both hands. In contrast, the non-hypertensive/hypertensive subjects control group demonstrates a higher arterial stiffness in the hypertensive subjects, which readily affects the pressing process of the robotic finger (Milkovich et al., 2022). However, when the number of channels is limited to a single or few, analyzing these situations becomes challenging. Consequently, the most crucial aspect for analyzing the arterial characteristics of the subjects through sensors is increasing the sensor channels.

5 Conclusion

In scenarios involving single or few-channel sensors, pressing offsets have substantial impacts on measurement results. By detecting whether there are any offsets occurring during the

pressing process, operators can adjust the pressing position to ensure the acquisition of 3DPis that accurately reflect the arterial conditions. This study discovers the pressing offsets in multi-channel pulse signals and analyzes the relationship between the pressing offsets and T_2 using a method to qualify the pressing offsets in pulse signal acquisition. First, we design a data acquisition system to capture 3DPis from the subjects. Second, the $errorT_2$ Stacked Surface ($errorT_2SS$) and the average error T_2 ($\overline{errorT_2}$) are proposed to qualify the pressing offsets in the tactile sensors. Finally, the subjects are divided into several control groups for subsequent analysis. The comparative study for $errorT_2SS$ exhibits a central low and peripheral high pattern. Furthermore, the error values increased as distance from the artery increased, particularly at the axial ends of the blood flow direction. For every 1 mm increase in distances between sensing elements and center sensing elements, the weighted $errorT_2$ in the radial direction escalates by 4.87%. When the distance is greater than 3.42 mm, the weighted radial $errorT_2$ experience sudden increases for all



subjects and control groups. The weighted error T_2 tends to be stable in the axial direction. The subjects in this study are middle-aged and elderly subjects aged 40–80 years, leading to a potential lack of representativeness. In the future, several enhancements may be contemplated for application in subsequent research. In the end, it remains imperative to highlight the necessity of increasing the sensor channels.

6 Limitation

Although this study discovers pressing offsets in radial pulse signal acquisition, some limitations should be reported. The subjects in this study are middle-aged and elderly subjects aged 40–80 years, leading to a potential lack of representativeness. The subjects aged 40–80 years may hinder the generalization of the methods presented in this study to younger subjects. In addition, the presence of missing data in error T_2 SS for female subjects is due to the weighted error T_2 absence of these regions, which may potentially affect the analysis of pressing offsets in female subjects, thereby hindering the acquisition of accurate conclusions. More young subjects and female subjects should be

included. In terms of prospects, several enhancements may be contemplated for application in subsequent research. For instance, broaden the age range of the sample population and include more control groups, such as subjects with other diseases, before and after exercise, and different postures, to make the research more universally applicable to the physical characteristics of blood vessels. In addition to expanding the composition of the sample, incorporating real-time measurement adjustments based on pressing offsets could serve as a potential future research enhancement.

Data availability statement

The raw data supporting the conclusion of this article will be made available by the authors, without undue reservation.

Ethics statement

The studies involving humans were approved by the National Cheng Kung University Hospital (Approval Number: B-ER-103-

263). The studies were conducted in accordance with the local legislation and institutional requirements. The participants provided their written informed consent to participate in this study.

Author contributions

CC: Methodology, Writing—original draft, Writing—review and editing. ZC: Methodology, Validation, Writing—review and editing. HL: Methodology, Writing—review and editing. BP: Data curation, Supervision, Writing—review and editing. YH: Validation, Writing—review and editing. XX: Supervision, Writing—review and editing. HX: Data curation, Writing—review and editing. XL: Data curation, Writing—review and editing.

Funding

The author(s) declare financial support was received for the research, authorship, and/or publication of this article. This work

References

- Alghatrif, M., Strait, J., Morrell, C., Canepa, M., Wright, J., Elango, P., et al. (2013). Longitudinal trajectories of arterial stiffness and the role of blood pressure: the Baltimore longitudinal study of aging. *Hypertension* 62, 934–941. doi:10.1161/hypertensionaha.113.01445
- Campitelli, R., Ferrario, M., Su, F., Creteur, J., Herpain, A., and Carrara, M. (2023). Pulse wave analysis as a tool for the evaluation of resuscitation therapy in septic shock. *Physiol. Meas.* 44, 105002. doi:10.1088/1361-6579/acfc94
- Candès, E. J., Li, X., Ma, Y., and Wright, J. (2011). Robust principal component analysis? *J. ACM* 58, 1–37. doi:10.1145/1970392.1970395
- Chen, G., Au, C., and Chen, J. (2021). Textile triboelectric nanogenerators for wearable pulse wave monitoring. *Trends Biotechnol.* 39, 1078–1092. doi:10.1016/j.tibtech.2020.12.011
- Chen, Z., Peng, B., Zhou, Y., Hao, Y., and Xie, X. (2023). Interpretable and accurate curve-fitting method for arterial pulse wave modeling and decomposition. *Int. J. Numer. Method Biomed. Eng.* 39, e3775. doi:10.1002/cnm.3775
- Chung, Y.-F., Hu, C.-S., Luo, C.-H., Yeh, C.-C., Si, X.-C., Feng, D.-H., et al. (2012). Possibility of quantifying TCM finger-reading sensations: II. An example of health standardization. *Eur. J. Integr. Med.* 4, e263–e270. doi:10.1016/j.eujim.2012.03.004
- Chung, Y. F., Hu, C. S., Yeh, C. C., and Luo, C. H. (2013). How to standardize the pulse-taking method of traditional Chinese medicine pulse diagnosis. *Comput. Biol. Med.* 43, 342–349. doi:10.1016/j.combiomed.2012.12.010
- Chung, Y., Hu, C., Chu, Y., Luo, C., and Si, X. (2011). “Exploring the conventional pulse conditions using Bi-sensing pulse diagnosis instrument,” in 4th International Conference on Biomedical Engineering and Informatics, Shanghai, China (IEEE).
- Cui, J., Tu, L., Zhang, J., Zhang, S., Zhang, Z., and Xu, J. (2019). Analysis of pulse signals based on array pulse volume. *Chin. J. Integr. Med.* 25, 103–107. doi:10.1007/s11655-018-2776-y
- Dario, P., and Bergamasco, M. (1988). An advanced robot system for automated diagnostic tasks through palpation. *IEEE Trans. Biomed. Eng.* 35, 118–126. doi:10.1109/10.1349
- Dario, P., and Buttazzo, G. (2016). An anthropomorphic robot finger for investigating artificial tactile perception. *Int. J. Robotics Res.* 6, 25–48. doi:10.1177/027836498700600302
- Deora, S., Sharma, S. K., Choudhary, R., Kaushik, A., Garg, P. K., Khera, P. S., et al. (2022). Assessment and comparison of distal radial artery diameter in anatomical snuff box with conventional radial artery before coronary catheterization. *Indian Heart J.* 74, 322–326. doi:10.1016/j.ihj.2022.06.007
- Fearing, R. S. (2016). Tactile sensing mechanisms. *Int. J. Robotics Res.* 9, 3–23. doi:10.1177/027836499000900301
- Francque, S., Van Der Graaff, D., and Kwanten, W. (2016). Non-alcoholic fatty liver disease and cardiovascular risk: pathophysiological mechanisms and implications. *J. Hepatology* 65, 425–443. doi:10.1016/j.jhep.2016.04.005
- Fu, Y., Zhao, S., and Zhu, R. (2019). A wearable multifunctional pulse monitor using thermosensation-based flexible sensors. *IEEE Trans. Biomed. Eng.* 66, 1412–1421. doi:10.1109/tbme.2018.2873754

was partially funded by National Natural Science Foundation of China, grant number 62071497.

Conflict of interest

The authors declare that the research was conducted in the absence of any commercial or financial relationships that could be construed as a potential conflict of interest.

Publisher’s note

All claims expressed in this article are solely those of the authors and do not necessarily represent those of their affiliated organizations, or those of the publisher, the editors and the reviewers. Any product that may be evaluated in this article, or claim that may be made by its manufacturer, is not guaranteed or endorsed by the publisher.

He, L., Luo, C., Xie, X., and Peng, B. (2019). “De-noising of 3D pulse images by channel-weighted robust principal component analysis,” in 2019 IEEE 11th International Conference on Advanced Infocomm Technology IEEE (IEEE).

Hu, C. S., Chung, Y. F., Yeh, C. C., and Luo, C. H. (2012). Temporal and spatial properties of arterial pulsation measurement using pressure sensor array. *Evid. Based Complement. Altern. Med.* 2012, 1–9. doi:10.1155/2012/745127

Huang, Y. C., Chang, Y. H., Cheng, S. M., Lin, S. J., Lin, C. J., and Su, Y. C. (2019). Applying pulse spectrum analysis to facilitate the diagnosis of coronary artery disease. *Evid. Based Complement. Altern. Med.* 2019, 2709486. doi:10.1155/2019/2709486

Jin, C., Xia, C., Zhang, S., Wang, L., Wang, Y., and Yan, H. (2019). A wearable combined wrist pulse measurement system using airbags for pressurization. *Sensors (Basel)* 19, 386. doi:10.3390/s19020386

Kim, J. U., Jeon, Y. J., Kim, Y. M., Lee, H. J., and Kim, J. Y. (2012). Novel diagnostic model for the deficient and excess pulse qualities. *Evid. Based Complement. Altern. Med.* 2012, 563958. doi:10.1155/2012/563958

Kim, J. U., Jeon, Y. J., Lee, Y. J., Kim, K. H., and Kim, J. Y. (2011). Novel diagnostic algorithm for the floating and sunken pulse qualities and its clinical test. *Evid. Based Complement. Altern. Med.* 2011, 1–10. doi:10.1155/2011/813427

Kong, K., Lau, W., Wong, B., Chan, H., Lee, B., Shen, B., et al. (2016). “A pulse-sensing robotic hand for tactile arterial palpation,” in 2016 IEEE International Conference on Cyber Technology in Automation, Control, and Intelligent Systems, Chengdu, China (IEEE).

Liu, Y. F., Wang, W., and Chen, X. F. (2023). Progress and prospects in flexible tactile sensors. *Front. Bioeng. Biotechnol.* 11, 1264563. doi:10.3389/fbioe.2023.1264563

Li, Z. (2007). “Design_and_Analysis_of_Improved_Butterworth_Low_Pass_Filter,” in 2007 8th International Conference on Electronic Measurement and Instruments, Xi’an, China (IEEE).

Luo, C.-H., and Chung, C.-Y. (2016). Non-invasive holistic health measurements using pulse diagnosis: II. Exploring TCM clinical holistic diagnosis using an ingestion test. *Eur. J. Integr. Med.* 8, 926–931. doi:10.1016/j.eujim.2016.06.016

Luo, C.-H., Chung, Y.-F., Hu, C.-S., Yeh, C.-C., Si, X.-C., Feng, D.-H., et al. (2012a). Possibility of quantifying TCM finger-reading sensations: I. Bi-sensing pulse diagnosis instrument. *Eur. J. Integr. Med.* 4, e255–e262. doi:10.1016/j.eujim.2012.03.003

Luo, C. H., Chung, Y. F., Yeh, C. C., Si, X. C., Chang, C. C., Hu, C. S., et al. (2012b). Stringlike pulse quantification study by pulse wave in 3D pulse mapping. *J. Altern. Complement. Med.* 18, 924–931. doi:10.1089/acm.2012.0047

Luo, C.-H., Su, C.-J., Huang, T.-Y., and Chung, C.-Y. (2016). Non-invasive holistic health measurements using pulse diagnosis: I. Validation by three-dimensional pulse mapping. *Eur. J. Integr. Med.* 8, 921–925. doi:10.1016/j.eujim.2016.06.017

Luo, C.-H., Ye, J.-W., Lin, C.-Y., Lee, T.-L., Tsai, L.-M., and Shieh, M.-D. (2018). L-cube polynomial for the recognition of normal and hypertensive string-like pulse mappings in Chinese medicine. *Inf. Med. Unlocked* 12, 27–33. doi:10.1016/j.imu.2018.05.006

- Luo, C. H., Zhang, Z., Peng, B., Xie, X., Lee, T. L., and Tsai, L. M. (2021). The novel three-dimensional pulse images analyzed by dynamic L-cube polynomial model. *Med. Biol. Eng. Comput.* 59, 315–326. doi:10.1007/s11517-020-02289-4
- Matsuzawa, Y., Kwon, T., Lennon, R., Lerman, L., and Lerman, A. (2015). Prognostic value of flow-mediated vasodilation in brachial artery and fingertip artery for cardiovascular events: a systematic review and meta-analysis. *J. Am. Heart Assoc.* 4, 959–960. doi:10.1016/j.jvs.2017.07.056
- Messas, E., Pernot, M., and Couade, M. (2013). Arterial wall elasticity: state of the art and future prospects. *Diagn. Interv. Imaging* 94, 561–569. doi:10.1016/j.diii.2013.01.025
- Milicevic, T., Katic, J., Milovac, S. N., Matetic, A., Aljinovic, J., Dogas, Z., et al. (2020). Auto-adaptive positive airway pressure improves lung function and arterial stiffness parameters in patients with severe obstructive sleep apnea syndrome over a 1 year follow-up. *Physiol. Meas.* 41, 125006. doi:10.1088/1361-6579/abcf5
- Milkovich, N., Gkousioudi, A., Seta, F., Suki, B., and Zhang, Y. (2022). Harmonic distortion of blood pressure waveform as a measure of arterial stiffness. *Front. Bioeng. Biotechnol.* 10, 842754. doi:10.3389/fbioe.2022.842754
- Munir, S., Guilcher, A., Kamalesh, T., Clapp, B., Redwood, S., Marber, M., et al. (2008). Peripheral augmentation index defines the relationship between central and peripheral pulse pressure. *Hypertension* 51, 112–118. doi:10.1161/hypertensionaha.107.096016
- Ohkuma, T., Ninomiya, T., Tomiyama, H., Kario, K., Hoshida, S., Kita, Y., et al. (2017). Brachial-ankle pulse wave velocity and the risk prediction of cardiovascular disease: an individual participant data meta-analysis. *Hypertension* 69, 1045–1052. doi:10.1161/hypertensionaha.117.09097
- Peng, B., Gong, K. F., Chen, Z. D., Chen, C., Zhang, Z., Xie, X. H., et al. (2022). Cross-Channel dynamic weighting RPCA: a de-noising algorithm for multi-channel arterial pulse signal. *Appl. Sciences-Basel* 12, 2931. doi:10.3390/app12062931
- Peng, B., Luo, C., Chan, W., Shieh, M., Su, C., and Tai, C. (2019). Development and testing of a prototype for 3D radial pulse image measurement and compatible with 1D pulse wave analysis. *IEEE Access* 7, 182846–182859. doi:10.1109/access.2019.2960338
- Qiao, L. J., Qi, Z., Tu, L. P., Zhang, Y. H., Zhu, L. P., Xu, J. T., et al. (2018). The association of radial artery pulse wave variables with the pulse wave velocity and echocardiographic parameters in hypertension. *Evid. Based Complement. Altern. Med.* 2018, 1–11. doi:10.1155/2018/5291759
- Rothermel, T. M., Win, Z., and Alford, P. W. (2020). Large-deformation strain energy density function for vascular smooth muscle cells. *J. Biomech.* 111, 110005. doi:10.1016/j.jbiomech.2020.110005
- Si, X.-C., Chu, Y.-W., Chung, Y., Hu, X.-S., Luo, C.-H., and Yeh, C.-C. (2011). “The wrist fixer system of three position and nine indicators pulse diagnosis instrument,” in 4th International Conference on Biomedical Engineering and Informatics.
- Song, X., Liu, Y., Wang, S., Zhang, H., Qiao, A., and Wang, X. (2023). Non-invasive hemodynamic diagnosis based on non-linear pulse wave theory applied to four limbs. *Front. Bioeng. Biotechnol.* 11, 1081447. doi:10.3389/fbioe.2023.1081447
- Su, C., Huang, T., and Luo, C. (2016). Arterial pulse analysis of multiple dimension pulse mapping by local cold stimulation for arterial stiffness. *IEEE Sensors J.* 16, 8288–8294. doi:10.1109/jsen.2016.2582805
- Tsai, Y. N., Huang, Y. C., Lin, S. J., Lee, S. M., Cheng, Y. Y., Chang, Y. H., et al. (2018). Different harmonic characteristics were found at each location on TCM radial pulse diagnosis by spectrum analysis. *Evid. Based Complement. Altern. Med.* 2018, 9018271–9018310. doi:10.1155/2018/9018271
- Visseren, F. L. J., Mach, F., Smulders, Y. M., Carballo, D., Koskinas, K. C., Back, M., et al. (2021). 2021 ESC Guidelines on cardiovascular disease prevention in clinical practice. *Eur. Heart J.* 42, 3227–3337. doi:10.1093/eurheartj/ehab484
- Wang, K. L., Cheng, H. M., Sung, S. H., Chuang, S. Y., Li, C. H., Spurgeon, H. A., et al. (2010). Wave reflection and arterial stiffness in the prediction of 15-year all-cause and cardiovascular mortalities: a community-based study. *Hypertension* 55, 799–805. doi:10.1161/hypertensionaha.109.139964
- Wang, D., Zhang, D., and Lu, G. (2016). A robust signal preprocessing framework for wrist pulse analysis. *Biomed. Signal Process. Control* 23, 62–75. doi:10.1016/j.bspc.2015.08.002
- Xu, B., Tu, S., Qiao, S., Qu, X., Chen, Y., Yang, J., et al. (2017). Diagnostic accuracy of angiography-based quantitative flow ratio measurements for online assessment of coronary stenosis. *J. Am. Coll. Cardiol.* 70, 3077–3087. doi:10.1016/j.jacc.2017.10.035
- Yang, T., Xie, D., Li, Z., and Zhu, H. (2017). Recent advances in wearable tactile sensors: materials, sensing mechanisms, and device performance. *Mater. Sci. Eng. R Rep.* 115, 1–37. doi:10.1016/j.mser.2017.02.001
- Yao, Y., Zhou, S., Alastruey, J., Hao, L., Greenwald, S. E., Zhang, Y., et al. (2022). Estimation of central pulse wave velocity from radial pulse wave analysis. *Comput. Methods Programs Biomed.* 219, 106781. doi:10.1016/j.cmpb.2022.106781
- Yf, C., Cs, H., Yw, C., Ch, L., and Xc, S. (2011). “Pulse differences and 3D PulseMappingin TPNI displacements,” in 4th International Conference on Biomedical Engineering and Informatics.
- Yuen, B., Dong, X., and Lu, T. (2019). Inter-patient CNN-lstm for QRS complex detection in noisy ECG signals. *IEEE Access* 7, 169359–169370. doi:10.1109/access.2019.2955738
- Zhang, Z., Peng, B., Luo, C.-H., and Tai, C.-C. (2021). ANFIS-GA system for three-dimensional pulse image of normal and string-like pulse in Chinese medicine using an improved contour analysis method. *Eur. J. Integr. Med.* 42, 101301–101309. doi:10.1016/j.eujim.2021.101301